Journal of Nuclear Materials 395 (2009) 50–57

Contents lists available at ScienceDirect

Journal of Nuclear Materials

journal homepage: www.elsevier.com/locate/jnucmat

MD simulation of atomic displacement cascades in Fe–10 at.%Cr binary alloy

M. Tikhonchev [a,b,*], V. Svetukhin [a], A. Kadochkin [a], E. Gaganidze [c]

[a] Ulyanovsk State University, Leo Tolstoy Str., 42, Ulyanovsk 432970, Russian Federation
[b] Joint Stock Company, "State Scientific Center Research Institute of Atomic Reactors", 433510 Dimitrovgrad-10, Russian Federation
[c] Forschungszentrum Karlsruhe, IMF II, 3640, D-76021 Karlsruhe, Germany

ARTICLE INFO

Article history:
Received 5 June 2009
Accepted 28 September 2009

PACS:
28.52.Fa
31.15.xvt
34.20.Cf
61.72.jd
61.72.jj
61.80.Hg

ABSTRACT

Molecular dynamics simulation of atomic displacement cascades up to 20 keV has been performed in Fe–10 at.%Cr binary alloy at a temperature of 600 K. The *N*-body interatomic potentials of Finnis–Sinclair type were used. According to the obtained results the dependence of "surviving" defects amount is well approximated by power function that coincides with other researchers' results. Obtained cascade efficiency for damage energy in the range from 10 to 20 keV is ≈0.2 NRT that is slightly higher than for pure α-Fe. In post-cascade area Cr fraction in interstitials is in range 2–5% that is essentially lower than Cr content in the base alloy. The results on size and amount of vacancy and interstitial clusters generated in displacement cascades are obtained. For energies of 2 keV and higher the defect cluster average size increases and it is well approximated by a linear dependence on cascade energy both for interstitials and vacancies.

1. Introduction

Reduced activation ferritic/martesitic (RAFM) 7–10%Cr-WVTa steels are primary candidate structural materials for the first wall (FW) and breading blanket (BB) structures of the future fusion power plants. Though RAFM steels gain some advantages over commercial alloys, low temperature hardening under neutron irradiation accompanied by embrittlement, decrease of impact toughness, and ductility still remain the principle obstacles for their application. Since the beginning of 2008 Ulyanovsk State University and Joint Stock Company, State Scientific Center Research Institute of Atomic Reactors (JSC SSC RIAR) jointly with Forschungszentrum Karlsruhe have set up a significant research project "High Dose Irradiation Damage of RAFM Steels". The designated project aims at understanding of the neutron irradiation damage in RAFM steels and its influence on their mechanical properties.

The present work concerns molecular dynamics (MD) simulation of atomic displacement cascades in Fe–10 at.%Cr binary alloy. The main goal is determination of some primary radiation damage parameters taking into consideration point defects recombination and clusterization in displacement cascades. The simulation is performed at a temperature of 600 K that approximately corresponds to irradiation temperature of RAFM steel specimens in BOR-60 (JSC SSC RIAR, Dimitrovgrad, Russia) within ARBOR-1 and ARBOR-2 irradiation programmes [1,2].

MD method is the most appropriate tool of atomic displacement cascade simulation being used by different research groups for simulation of irradiation damage in various materials. Particularly, pure α-Fe has been extensively studied by using of different potentials of interatomic interaction. Cascade simulation in alloys is also being widely performed, though the problem of proper potential development for multicomponent systems still remains. Recently a number of works dedicated to Fe–Cr alloys have been published [3–6]. Malerba et al. [3] carried out a dynamic simulation of displacement cascades of Fe–10%Cr alloy for the primary knock-on atom (PKA) energies up to 15 keV. Later on Terentyev et al. [4] performed calculations for PKA energies up to 50 keV. Wallenius et al. [5] simulated cascades for Fe–5%Cr and Fe–20%Cr systems. The authors in [3–5] make use of interatomic potentials resting on embedded atom method (EAM). However, Fe potential used in [3,4] reveals the ⟨1 1 1⟩ dumbbell structure for interstitial atoms to be more stable than ⟨1 1 0⟩ one, that contradicts experimental data and results of ab initio calculations. The potentials used in [5] happens to yield formation energies of mixed Fe–Cr "dumbbell" in α-Fe matrix twice as large as ab initio calculations.

Shim et al. [6] had performed MD simulations of displacement cascades up to 20 keV in Fe and Fe–10 at.%Cr using two different parameterizations of Finnis–Sinclair type interatomic potentials. In particular, they had shown that the quantity of mixed Fe–Cr dumbbells is sensitive to the choice of Fe–Cr cross-potential.

* Corresponding author. Address: Ulyanovsk State University, Leo Tolstoy Str., 42, Ulyanovsk 432970, Russian Federation. Tel./fax: +7 8422675054.
E-mail address: tikhonchev@sv.ulsu.ru (M. Tikhonchev).

0022-3115/$ - see front matter © 2009 Elsevier B.V. All rights reserved.
doi:10.1016/j.jnucmat.2009.09.015

2. Simulation method and interatomic potentials

For displacement cascade simulation we made use of MD method and FRENKLOW code [7] that was developed in Tver polytechnic university and subsequently modified by our researchers. Displacement cascade simulation starts from imparting an initial velocity in a chosen crystallographic direction to one of crystallite atoms (PKA) and continues till perturbation cools down. In doing so, it is essential to consider different non-equivalent PKA momentum directions.

For the performed simulation, a semi-empirical manybody potential of interatomic interaction is applied. By using *N*-body potential each atom's energy is rather represented as some function of its local surrounding than constitutes the sum of pair interactions. Several construction schemes of such potential were developed for metals: embedded atom method [8], Finnis–Sinclair scheme [9], and Rosato–Guellopé–Legrand scheme [10]. Though physical interpretations are slightly different, all these methods yield the same analytic equation for *N* particles system's total energy.

$$E_{tot} = \sum_{i=1}^{N} F_i(\rho_i) + \sum_{i=1}^{N-1} \sum_{j=i+1}^{N} \varphi_{ij}(r_{ij}), \tag{1}$$

$$\rho_i = \sum_{\substack{j=1 \\ (j\neq i)}}^{N} \psi_j(r_{ij}), \tag{2}$$

where E_{tot} is crystal energy, ρ_i in EAM formalism is the electron density at cite i generated by other atoms, $F_i(\rho_i)$ is energy of embedding of atom i into electron liquid with density ρ_i, $\psi_j(r_{ij})$ is electron density of atom j as a function of distance to its center, r_{ij} is distance between i and j atoms and $\varphi_{ij}(r_{ij})$ is pairwise interatomic potential between i and j atoms.

When constructing pairwise potential it is common to divide it into three parts (see, for instance [11]): *equilibrium*, *high-energy* and *intermediate*. The *equilibrium* part of pair potential is designated to explain interactions on interatomic distances close to or greater than the distance between the nearest neighbours in an equilibrium crystal. This part ($\varphi_{equilibrium}(r)$) may have different analytic forms for both different atoms and different methods and approaches used in potential construction.

The *high-energy* part describes interatomic interactions at short distances (typically up to 1 Å). This potential part is repulsive (i.e. decreasing with r) and it is usually described by the equation:

$$\varphi_{short\text{-}dist}(r) = \frac{Z_1 Z_2 e^2}{4\pi\varepsilon_0 r} \Phi\left(\frac{r}{a}\right), \tag{3}$$

where Z_i is atom number, e is electron charge, ε_0 is the dielectric constant, a is defined here according to Biersack and Ziegler approach [40]

$$a = \frac{0.88534 \times a_0}{\sqrt{Z_1^{2/3} + Z_2^{2/3}}}, \tag{4}$$

with $a_0 = 0.529$ Å being Bohr radius and $\Phi(x)$ being screening function given by:

$$\Phi(x) = 0.1818e^{-3.2x} + 0.5099e^{-0.9423x} + 0.2802e^{-0.4029x} + 0.02817e^{-0.2016x}. \tag{5}$$

The *intermediate* part is designated to smoothly join *equilibrium* and *high-energy* parts so that $\varphi(r)$ function and its first derivative should be continuous. In the present work the intermediate part is represented as:

$$\varphi_{join}(r) = e^{(B_0 + B_1 r + B_2 r^2 + B_3 r^3)}, \quad r_1 \leqslant r \leqslant r_2, \tag{6}$$

where $[r_1, r_2]$ is a "join" section, B_i parameters are chosen so that the equations

$$\varphi_{join}(r_2) = \varphi_{equilibrium}(r_2),$$

$$\varphi'_{join}(r_2) = \varphi'_{equilibrium}(r_2),$$

$$\varphi_{join}(r_1) = \varphi_{short\text{-}dist}(r_1),$$

$$\varphi'_{join}(r_1) = \varphi'_{short\text{-}dist}(r_1)$$

should be satisfied.

In the present work for Fe we used *N*-body potential of Finnis–Sinclair type from Ackland et al. [12], which is derived from potential 2 from [13] by embedding function modification. The boundaries of the intermediate region for a pairwise potential part is given by $r_1 = 1$ Å, $r_2 = 2.05$ Å. High-energy and joint parts correspond to Eqs. (3)–(6). Cutting radius is 5.3 and 4.2 Å for φ and ψ functions, respectively.

It is noteworthy that, the used potential is constructed so that the more stability should be provided for ⟨1 1 0⟩ "dumbbell" configuration than for ⟨1 1 1⟩ one. The difference between corresponding formation energies is ~0.5 eV that agrees well with experimental results on α-Fe [21].

We use Finnis–Sinclair potential [9] for Cr:

$$\psi_{CrCr}(r) = \begin{cases} A^2((r-d)^2 + b(r-d)^3/d), & r \leqslant d \\ 0, & r > d \end{cases}, \tag{7}$$

$$F_{CrCr}(\rho) = -\sqrt{\rho}, \tag{8}$$

$$\varphi_{CrCr\_equilibrium}(r) = \begin{cases} (r-C)^2(C_0 + C_1 r + C_2 r^2), & r \leqslant C \\ 0, & r > C \end{cases}. \tag{9}$$

The potential parameters are given in Table 1. It is noteworthy that the potential yields a slightly positive Cauchy pressure $(C_{12}-C_{44})/2 \approx 1.35 \times 10^9$ Pa which disagree with experiment [22] where negative Cauchy pressure for Cr is obtained. However, as it is noted in [5] with reference to paper [23], at temperatures above 450 K chromium is paramagnetic and has a positive Cauchy pressure. For using this potential in displacement cascade simulation when the distance between atoms becomes small, it is reasonable to modify $\psi_{CrCr}(r)$ function. The matter is that it increases at $r < d(1-2/(3b)) \approx 2.465$ Å and, moreover, it is negative at $r < (1-1/b)d \approx 1.74$ Å. Therefore, for $r \leqslant r_0 = 2.498$ Å we assumed.

$$\psi_{CrCr}(r) = A^2((r-d)^2 + b(r-d)^3/d) + k(r_0 - r)^3, \quad r \leqslant r_0, \tag{10}$$

where $k = 11.1$ eV/Å^3. Original and modified curves of $\psi_{CrCr}(r)$ function are given in Fig. 1. *High-energy* and *intermediate* parts of $\varphi_{CrCr}(r)$ function were determined in accordance with Eqs. (3)–(6) with r_1 and r_2 values coinciding with those of Fe (i.e. 1 and 2.05 Å, respectively).

To test chosen potentials for Fe and Cr we carried out calculations of atom displacement threshold energies and performed comparison of the obtained values with the experimental data. bcc Fe and Cr crystallites comprising nearly 10,000 atoms were used to calculate displacement threshold energy (E_d). Calculations were done with periodic boundary conditions. The initial crystallite temperature was 0 K. When determining threshold energy the search of stable configurations starts from low PKA energies,

Table 1
Potential parameters for Cr (all distances are expressed in Å and energies in eV).

A	1.453418	d	3.915720	C_0	29.1429813	C_2	4.7578297
b	1.8	C	2.90	C_1	−23.3975027		

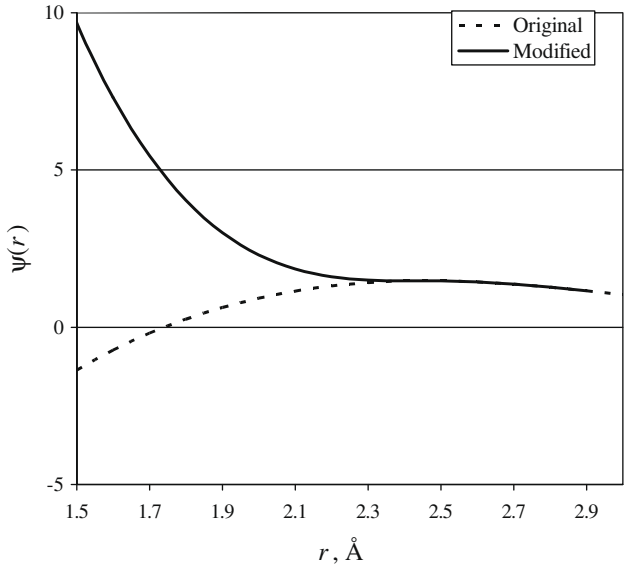

Fig. 1. Original and modified function $\psi_{CrCr}(r)$.

that result formation of unstable displacements at the initial stage of calculation. Gradual increase of PKA energy enables us to define energy at which stable Frenkel pairs form. We increased the PKA energy with a step of 1 eV. Thus, the error in E_d determination for a fixed crystallographic direction caused by discrete PKA energy change does not exceed 1 eV. Noteworthy, a step-by-step method of energy increase should not be replaced by a binary search method, since the observation of formation of stable Frenkel pair at some PKA energy does not guarantee formation of such a pair at a higher energy.

Unfortunately, there are few experimental results on bcc Fe and Cr threshold displacement energies obtained by the irradiation of monocrystal foil by electrons. Furthermore, according to works [24–26] such experiments are unlikely to obtain reliable data. In particular, low-energy threshold for some directions may be initiated by electrons travelling along the inclined line towards these directions. Thus, reliable results can be obtained only for a minimum E_d value that is 16–20 eV for bcc Fe and 21–28 eV for Cr, and that correspond to crystallographic direction near ⟨1 0 0⟩ for both elements.

The comparison of E_d values calculated by us with known experimental results are given in Table 2. In accordance with method [27] we defined threshold energy for a given crystallographic direction as a minimum value among all calculated E_d values for all possible directions deflecting from a given direction by up to 20°. The E_d values obtained by us agree well with most of experimental results. Considerable discrepancy is revealed only for ⟨1 1 1⟩ direction for Fe. There is also a substantial discrepancy (8 eV) in experimental data on minimum value of E_d for Cr.

Note, that E_d values for bcc Fe calculated in this work slightly differ from those obtained in [27] with the same interatomic potential. In a latter case 17, 33 and 33 eV for ⟨1 0 0⟩, ⟨1 1 0⟩ and ⟨1 1 1⟩, respectively, and 15 eV as a minimum value were obtained.

When calculating damage dose the value of so called average threshold displacement energy $\overline{E}_d$ plays a key role.This energy can be determined in different ways [27]. The most common way is a determination of an arithmetical mean of threshold displacement energies observed for each of the considered directions. To assess $\overline{E}_d$ we calculated threshold displacement energies for different PKA impulse directions assigned by the simulation of an isotropic random vector. The obtained values are presented in Table 2 as well. Both our assessments are close to the currently used $\overline{E}_d$ = 40 eV value recommended by ASTM standard for determination of damage dose in these materials [33]. The corresponding assessments from paper [4] are presented in Table 2 as well. Note that potential for Fe used in [4] gives high estimates for ⟨1 1 0⟩ direction and for averaged threshold displacement energy.

To obtain $\psi_{FeCr}(r)$ and $\varphi_{FeCr\_equilibrium}(r)$ cross-potentials the scheme offered by Konishi et al. [34] was used:

$$\psi_{FeCr} = \alpha\sqrt{\psi_{FeFe}\psi_{CrCr}}, \tag{11}$$

$$\varphi_{FeCr\_equilibrium} = \frac{\beta}{2}\left(\frac{\psi_{FeCr}}{\psi_{FeFe}}\varphi_{FeFe\_equilibrium} + \frac{\beta}{2}\frac{\psi_{FeCr}}{\psi_{CrCr}}\varphi_{CrCr\_equilibrium}\right) \tag{12}$$

where α and β are adjustable parameters.

α and β parameters were chosen in accordance with a formation energy of a binary Fe–10%Cr alloy and formation energy of Fe–Cr "dumbbells" directed towards ⟨1 1 0⟩ and ⟨1 1 1⟩ ($E^f_{Fe-Cr\langle 110\rangle}$ and $E^f_{Fe-Cr\langle 110\rangle}$, respectively) in bcc Fe. Formation energy ΔH_f of Fe–Cr ferromagnetic alloy with randomly orientated atoms were calculated by Olsson et al. [35] in terms of EMTO ab initio method for Cr concentrations from 2 to 20 at.%. They obtained ΔH_f = 0.0104 eV for Fe–10 at.%Cr alloy. For formation energies of Fe–Cr "dumbbell" we used the results of VASP ab initio calculations from [36]. α and β parameters were chosen so that they should satisfy ΔH_f = 0.0104 eV and provide minimum of a maximum absolute deviation of $E^f_{Fe-Cr\langle 110\rangle}$ and $E^f_{Fe-Cr\langle 111\rangle}$ values from corresponding results in VASP calculations. The parameters are the following:

$$\alpha = 1.02135, \quad \beta = 1.06743.$$

Cut-off radius for $\psi_{FeCr}(r)$ and $\varphi_{FeCr\_equilibrium}(r)$ functions is r_c = 3.91572 Å. In this case $\lim_{r\to r_c-0}\frac{d\psi_{FeCr}}{dr} \neq 0$. Therefore at r $[r_c - \Delta r, r_c]$, where Δr = 0.2 Å, we multiplied $\psi_{FeCr}(r)$ by polynomial $P_3(r) = a_1r^3 + a_2r^2 + a_3r + a_4$, where $a_1 = -98.85126206$ Å^{-3}, a_2 = 1096.681087 Å^{-2}, $a_3 = -4055.52757$ Å^{-1}, a_4 = 5000.

The graphs of original and modified function $\psi_{FeCr}(r)$ are given Fig. 2. Table 3 comprises $E^f_{Fe-Cr\langle 110\rangle}$ and $E^f_{Fe-Cr\langle 111\rangle}$ values calculated with the used potential and substitution energy of one Fe atom by Cr atom in bcc Fe (E^s_{Cr}) along with the appropriate results of VASP calculations. Table 3 also includes values calculated by means of Farkas potential [37] and Fe–5Cr and Fe–20Cr potentials from [5] (the two latter potentials are developed for Cr fraction in alloys of 5% and 20%, respectively). According to our results $E^f_{Fe-Cr\langle 110\rangle} < E^f_{Fe-Cr\langle 111\rangle}$, that substantially contradicts the results of VASP calculations. Similar discrepancy is observed in Fe–5Cr and Fe–20Cr potentials. However, in comparison with other potentials, the potential offered in the current work yields results most close to those of VASP results.

3. Displacement cascades simulations

For displacement cascades simulation and for assessment of the number of "survived" defects, bcc Fe–10 at.%Cr crystallites with up to ≈600,000 atoms were used. The arrangement of different atoms in an alloy occurred at random, i.e. each crystallite atom was assigned type Fe with the probability of p = 0.9 or type Cr otherwise. For calculation we used periodic boundary conditions. Therefore, in order to avoid fast cyclicity of perturbance along close-packed ⟨1 1 1⟩ direction, crystallites were used in a form of a rectangular parallelepiped rather than a cube. Simulation was done at the initial crystallite temperature of T = 600 K for eight various PKA energies (E_{PKA}): 0.1, 0.5, 1, 2, 5, 10, 15 and 20 keV. Lattice constant a_0 = 2.8753 Å was obtained for considered alloy from MD simulation of isothermal–isobaric NPT-ensemble at temperature of 600 K. The initial temperature was assigned by imparting the

Table 2
Calculated and experimental data on threshold displacement energies, eV.

		Minimum value	Crystallographic direction			$\bar{E}_d$
			⟨1 0 0⟩	⟨1 1 0⟩	⟨1 1 1⟩	
Fe	Calculation					
	– Present work	18	18	29	28	38.9 ± 1.5
	– [4]		20	48	30	54.5 ± 0.5
	Experiment					
	– [28]	17	17	>30	20	
	– [29]	20	20	30	–	
	– [30]	16–18	–	–	–	
Cr	Calculation					
	– Present work	18	18	35	24	46.2 ± 1.5
	– [4]		16	34	28	44.2 ± 0.4
	Experiment					
	– [31]	21	21	34	24	
	– [24] (with the reference to [32])	28	–	–	–	

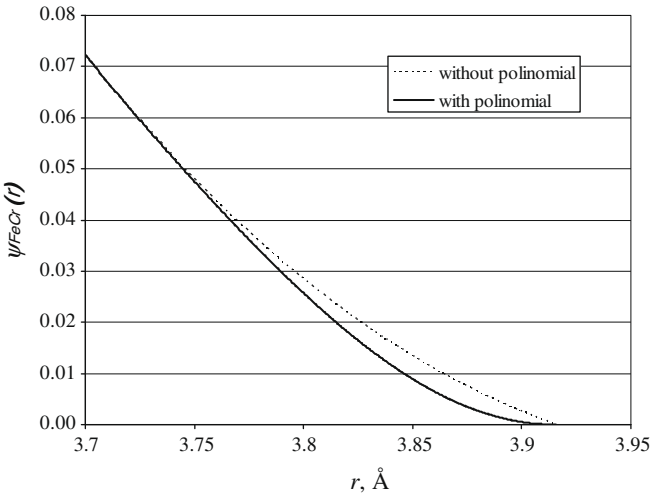

Fig. 2. The original and modified function $\psi_{FeCr}(r)$.

random initial velocities to crystallite atoms with further MD simulation during 1 ps with 1 fs time step. For each PKA energy a cascade for 17 various directions was simulated so that approximately the whole region of all directions should be covered (taking into consideration crystal symmetry). The choice of that approach allows obtaining more precise average evaluations than simulation of statistically random directions because statistics is rather small (17 directions) and the significant increase in the number of directions requires significant computational power. The list of the considered directions is given in Table 4.

In cascade modelling no algorithms of kinetic energy decrease were used to imitate crystal's cooling down, i.e. computational box was in adiabatic condition because of periodic boundary conditions. Temperature rise of crystallite is from ≈ 16 K for $E_{PKA} = 0.1$ keV up to 123.8 K for $E_{PKA} = 20$ keV. Calculations were

Table 3
Formation energies of the single mixed ⟨1 1 0⟩ and ⟨1 1 1⟩ Fe–Cr dumbbells in an iron matrix and substitution energy E^s_{Cr} of a single Cr atom, eV.

	$E^f_{Fe-Cr\langle 110\rangle}$	$E^f_{Fe-Cr\langle 111\rangle}$	E^s_{Cr}
Present work	2.76	3.00	0.02
VASP [36]	3.06	2.7	−0.35
Farkas et al. [37]	4.31	4.24	0.7
Fe–5Cr [5]	7.63	7.66	0.18
Fe–20Cr [5]	8.19	8.39	0.46

Table 4
Directions of PKA momentum in polar coordinates (angle φ is counted from ⟨1 0 0⟩ direction in (0 0 1) plane, angle θ is counted from ⟨0 0 1⟩ direction).

N	θ (degree)	φ (degree)	N	θ (degree)	φ (degree)
1	9	22.5	10	63	22.5
2	27	11.25	11	63	31.5
3	27	33.75	12	63	40.5
4	45	5.625	13	81	4.5
5	45	16.875	14	81	13.5
6	45	28.125	15	81	22.5
7	45	39.375	16	81	31.5
8	63	4.5	17	81	40.5
9	63	13.5			

done with an uneven time step chosen so that it should not exceed 10^{-3} ps. Moreover, atom with maximal kinetic energy should not be shifted by more than 0.02 Å within one time step.

The simulated time of cascade formation was chosen so that the simulation of the whole process of defect formation and relaxation should proceed until its cooling down. Data on crystallite's size and simulated time are given in Table 5.

During displacement cascades simulation the analysis of crystallite was done, the number of defects that experience recombination in a cascade was calculated, and the average number of such defects for each PKA energy was determined. Count of defects in a crystallite was performed in the following way. Each *i*-site of an ideal crystal lattice was connected with Wigner–Seitz cell which is defined as a set of all space points such as the distance between these points and *i*-site is less or equal (taking into consideration periodic boundary conditions) than the distance to any other lattice site. Atom deficiency in C_i cell is interpreted as a vacancy in *i*-site, the presence of more than one atom in C_i cell is assumed to be the interstitial near *i*-site. The number of defects is defined as a total amount of Wigner–Seitz cells not containing any of material atoms. Fig. 3 shows calculated average defect number in crystallite as a function of the time of cascade development for 3 PKA energies: 1, 10, and 20 keV. For PKA energy of 20 keV the number of Frenkel pairs at the peak of ballistic stage is about 3500 that is almost four times as high as corresponding result from paper [6].

The part of "survived" defects was determined by the following equation:

$$p(E_{PKA}) = \frac{N(E_{PKA})}{f(E_{PKA})}, \tag{13}$$

where $N(E_{PKA})$ is calculated average account of "survived" defects, $f(E_{PKA}) = 0.8E_{PKA}/(2\ \bar{E}_d)$ is an account of atomic displacements

Table 5
Crystallite size, number of simulated atoms and time step for different PKA energies.

Energy PKA (keV)	Crystallite size $l_x \times l_y \times l_z$ (Å)	Number of crystallite's atoms	Simulated time (ps)
0.1	69.0072 × 63.2566 × 66.1319	24,288	10
0.5	109.2614 × 103.5108 × 106.3861	101,232	12
1	123.6379 × 117.8873 × 120.7626	148,092	14
2	135.1391 × 129.3885 × 132.2638	194,580	16
5	155.2662 × 149.5156 × 152.3909	297,648	20
10	172.518 × 163.8921 × 169.6427	403,560	24
15	184.0192 × 178.2686 × 181.1439	499,968	28
20	195.5204 × 186.8945 × 192.6451	592,280	30

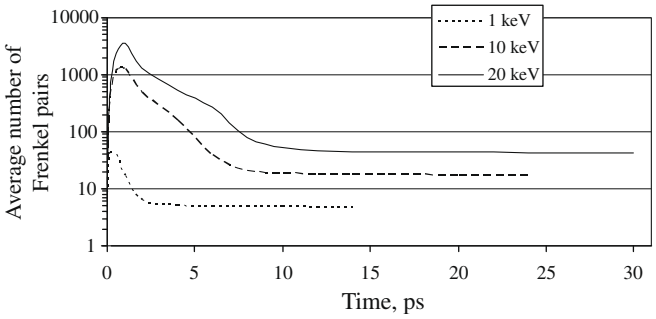

Fig. 3. Average number of Frenkel pairs versus simulation time of cascade evolution.

Table 6
Average number and the part of the "survived" defects.

E_{PKA} (keV)	$N(E_{PKA})$	$p(E_{PKA})$
0.1	0.94 ± 0.32	0.94 ± 0.32
0.5	3.18 ± 0.62	0.64 ± 0.13
1	4.59 ± 0.94	0.46 ± 0.09
2	5.94 ± 1.02	0.30 ± 0.05
5	13.00 ± 1.55	0.26 ± 0.03
10	17.35 ± 2.77	0.17 ± 0.03
15	28.47 ± 3.96	0.19 ± 0.03
20	41.82 ± 4.94	0.21 ± 0.03

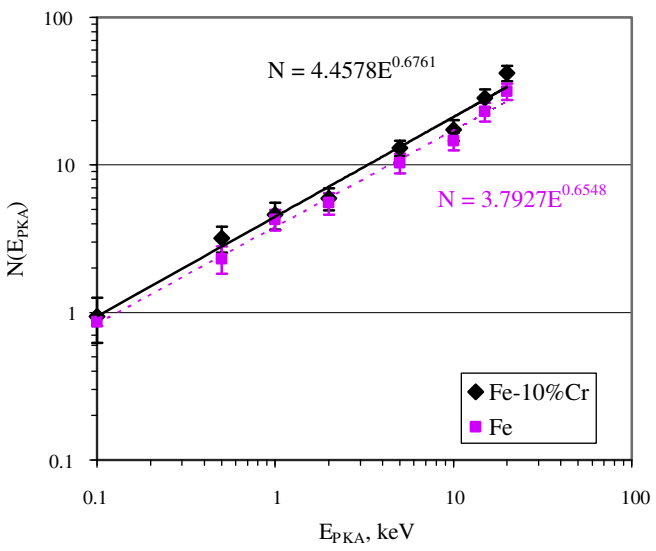

Fig. 4. Average number of surviving defects versus PKA energy.

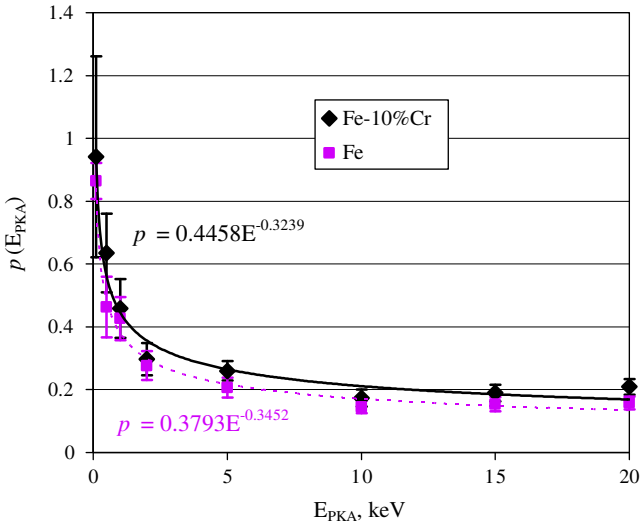

Fig. 5. Cascade efficiency versus PKA energy.

according to NRT-standard (without taking into account an inelastic losses of energy which are low in considered energy interval).

Value of $p(E_{PKA})$ is often referred to as a cascade efficiency in modern literature. The threshold displacement energy E_d=40 eV value was used here. The derived $N(E_{PKA})$ and $p(E_{PKA})$ values

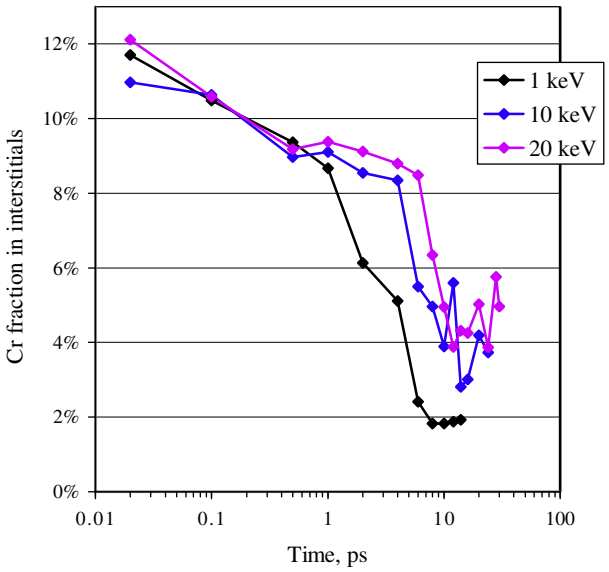

Fig. 6. Change of Cr content in interstitial atoms during cascade development.

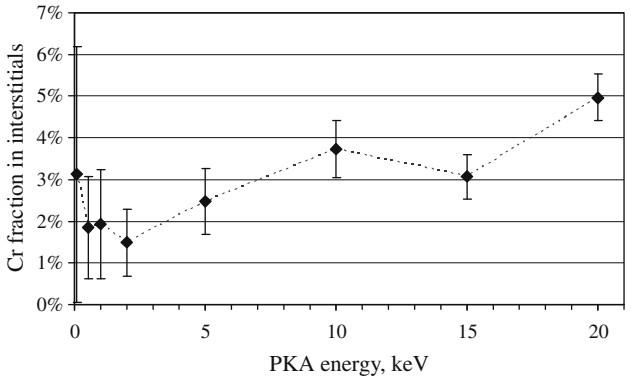

Fig. 7. Cr fraction in interstitials in post-cascade area versus PKA energy.

averaged over PKA momentum directions are given in Table 6 and in Figs. 4 and 5, respectively. From the obtained results the rise in defects number with the rising E_{PKA} is observed throughout the considered energy range. Though the amount of the defects survived recombination in cascade rises slightly with E_{PKA} greater than 10 keV, this value may be considered decreasing with E_{PKA} taking into consideration all errors.

Calculated values of $N(E_{PKA})$ and $p(E_{PKA})$ for both Fe–10 at.%Cr alloy being considered and pure α-Fe at the same initial temperature (T = 600 K) are given in Figs. 4 and 5.

Bacon et al. [38] and Wooding et al. [39] point that the dependence $N(E_{PKA})$ for metals is well described with power function of the following type:

$$N(E) = A \cdot E^{B} \tag{14}$$

The results obtained by us are well described by such type function (see Fig. 4) too, namely:

$$N(E) = 4.46 \cdot E^{0.68}, \quad \text{for} \quad \text{Fe—10 at.\%Cr}, \tag{15}$$

$$N(E) = 3.79 \cdot E^{0.65}, \quad \text{for Fe} \tag{16}$$

where E is PKA energy in keV.

Taking into consideration Eq. (13) we get the corresponding approximations for $p(E_{PKA})$ dependence from Eqs. (15) and (16):

$$p(E) = 0.446 \cdot E^{-0.32}, \quad \text{for Fe—10 at.\%Cr}, \tag{17}$$

$$p(E) = 0.379 \cdot E^{-0.35}, \quad \text{for Fe}, \tag{18}$$

The dependencies given by Eqs. (16) and (17) slightly differ from results of Terentyev et al. [4] who obtained for T = 300 K.

$$N(E) = 4.54 \cdot E^{0.87}, \quad \text{for Fe—10 at.\%Cr}, \tag{19}$$

$$N(E) = 4.05 \cdot E^{0.86}, \quad \text{for Fe}, \tag{20}$$

and of Shim et al. [6] who obtained for T = 673 K

$$N(E) = 3.47 \cdot E^{0.82}, \tag{21}$$

both for Fe–10 at.%Cr and pure Fe.

Cascade efficiency values assessed in [4] for E_{PKA} = 20 keV are approximately one and a half as large as our corresponding values. This distinction is rather caused by considerable difference in temperatures of the original crystallites.

The results on change of Cr fraction in interstitials during cascade development are given in Fig. 6. At the early stage of cascade formation Cr content in interstitials is 11–12% that slightly exceeds Cr content in the original alloy. At the next stage, however, a gradual decrease of Cr content down to 2–5% is observed that proves more intensive recombination of Cr interstitial atoms with vacancies compared to Fe atoms. Though in Fig. 6 we confined ourselves to presenting the results only for PKA energies 1, 10, and 20 keV, the results for the rest considered energies look similar. Fig. 7 shows Cr fraction in interstitial atoms at the final moment of modelling of cascade evolution. By this moment only small fraction of Cr–Cr "dumbbell" embeddings is observed in crystallite, most fraction of Cr interstitial atoms is concentrated in the mixed Fe–Cr "dumbbells".

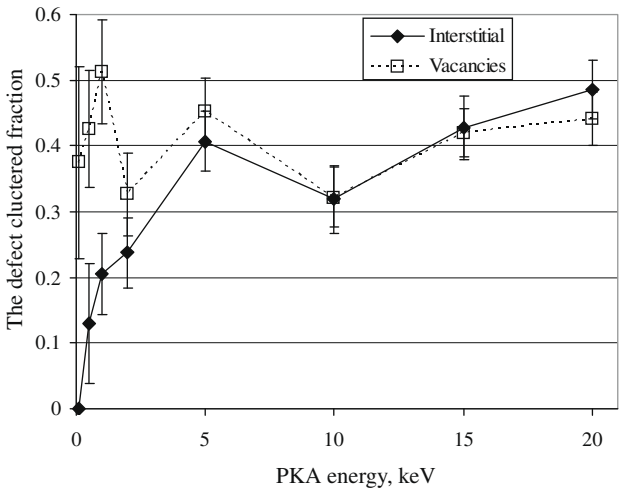

Fig. 8. The fraction of clustered defects versus PKA energy.

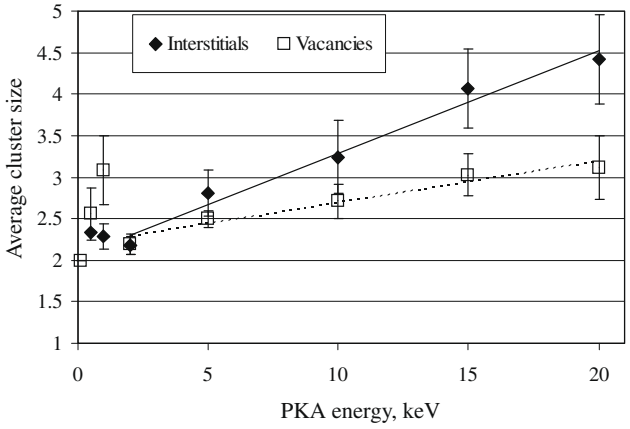

Fig. 9. Average size of defect cluster versus PKA energy.

The agglomeration of the produced point defects into clusters plays a key role in the material's microstructural evolution under irradiation. When modelling displacement cascades, we, along with the estimation of the number of "surviving" defects, performed the assessment of sizes and number of interstitial and vacancy clusters remaining in a crystallite after cascade damping. The defects of the same type were considered to belong to one cluster provided that the Wigner–Seitz cells corresponding to them had an area of a shared boundary. Since in our case crystal lattice has bcc structure, Wigner–Seitz cells have an area of a shared boundary only when the lattice sites corresponding to them are the first or second neighbours.

Fig. 8 shows calculated fraction of point defects forming clusters at the final stage of the cascade modelling for Fe–10 at.%Cr alloy. It is well seen that up to the PKA energies of 10 keV the number of the vacancies participating in clusterization exceeds the number of the interstitials included into clusters. At much higher energies

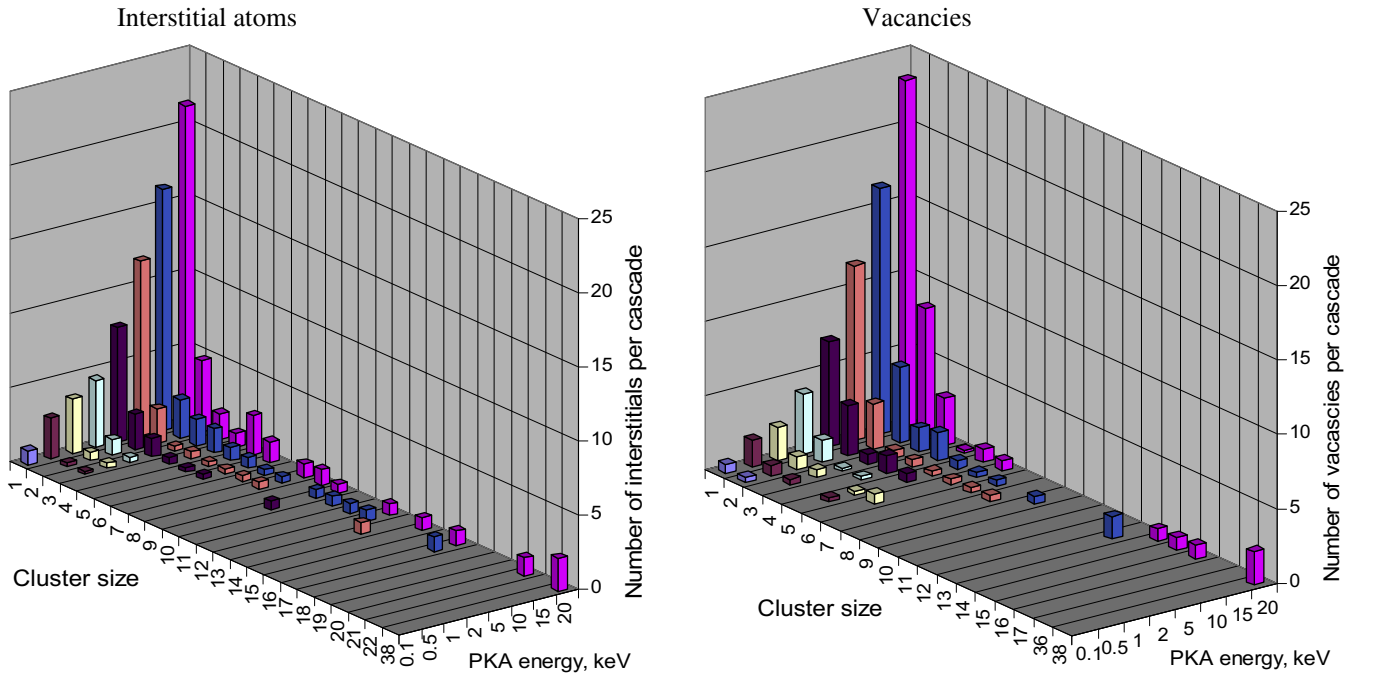

Fig. 10. The number of interstitials and vacancies in clusters per cascade as a function of PKA energy. The data were obtained by averaging over all cascades at each energy.

the number of the vacancies in clusters becomes less than the number of the interstitials forming clusters.

Fig. 9 shows the obtained data on average size of the interstitial and vacancy clusters. Cluster size is defined here as the number of defects in the cluster and all clusters of size 2 and higher are taken into account. The cluster size increases as PKA energy rises starting from 2 keV both for interstitial and vacancy clusters. Moreover, these values are well approximated by the linear function of E_{PKA} in energy range from 2 to 20 keV.

Fig. 10 shows two histograms representing distribution of the point defect cluster sizes at the final moment of cascade simulation. As it is seen from the histograms the number of defects gathering into large enough clusters rises in cascades for PKA energies between 15 and 20 keV. Thus, at E_{PKA} = 20 keV clusters comprising up to 38 defects for both vacancies and interstitial atoms are observed.

4. Discussion and conclusions

Simulation of atom displacement cascades in a binary Fe–10%Cr alloy for PKA energy range of 100 eV–20 keV is performed with MD method in the present work. For simulation *N*-body interatomic potentials of Finnis–Sinclair type were used. When choosing potentials for Fe and Cr and for preparation Fe–Cr cross-potentials we used an approach similar to that of [6]. However, using the same potential for Cr, in contrast to the [6] we modified it. Moreover, we used a newer potential for Fe. In preparing Fe–Cr potential (see Eqs. (12) and (13)) we, in particular, satisfied ab initio results of a binary Fe–10 at.%Cr alloy formation energy. Thus, the cross-potential obtained by us is suited for simulation of alloy with the given Cr concentration of 10%. Similar situation is observed, for instance in [5], where non-equivalent potentials for Cr concentration of 5% and 20% were prepared by means of embedded atom method for Fe–Cr system. For single component Fe and Cr systems the calculations of atom displacement threshold energies were performed. The comparison of the obtained results with the experimental results was performed to check the adequateness of the potentials being used. The obtained results are shown to be generally in agreement with the experiment. The obtained results of average displacement threshold energy (38.9 ± 1.5 and 46.2 ± 1.5 eV for Fe and Cr, respectively) are close to a standard value of 40 eV recommended by ASTM.

The dependence of the part of defects "surviving" in displacement cascades on PKA energy (in energy range from 0.1 to 20 keV) was calculated. According to the obtained results the dependence of the number of "surviving" defects is well approximated by power function that coincides with other researcher's results. Cascade efficiency value at E_{PKA} starting from 10 keV is ≈0.2. This value is close to the corresponding result from paper [6]. However, this value is lower than a respective value of ≈0.3 obtained in [4] for T = 300 K, and it exceeds the result of ≈0.135 from work [5] for T = 150 K. In both cases the discrepancies can be explained by substantially different crystallite temperature as well as by the use of different interatomic potentials. In particular, potential for Fe in [4] yields for greater dumbbell stability for ⟨1 1 1⟩ configuration than ⟨1 1 0⟩ one, that contradicts experimental data and ab initio calculations for α-Fe. Cross-potentials Fe–Cr in [5] produces much higher formation energies of mixed "dumbbell" Fe–Cr embeddings in α-Fe matrix. It is noteworthy that, both the number of "surviving" Frenkel pairs and the cascade efficiency value appear to be slightly larger for Fe–10%Cr system than for a pure Fe.

According to the obtained results Cr fraction in interstitials is 11–12% at the beginning stage of cascade evolution that exceeds slightly Cr fraction in an initial alloy. However, further a gradual decrease of Cr fraction down to 2–5% is observed. This result well agrees with results from [6] for FeCr I potential, but does not agree with results from the same paper for FeCr II potential as well as from paper [4] where Cr fraction in interstitials in post-cascade area lays in intervals 20–25% and 50–70%, respectively. Wallenius et al. [5] observed higher Cr concentration in interstitials than in a base alloy too. This discrepancy is likely to be the consequence of different potentials. To confirm or refute these results further investigations including experimental ones are required.

The results on size and number of vacancy and interstitial clusters generated in displacement cascades for different E_{PKA} are

obtained. In accordance with these results at E_{PKA} up to 10 keV the number of vacancies participating in clusterization exceeds the number of interstitials included into clusters. At much higher energies the number of vacancies in clusters becomes less than the number of interstitials, which form clusters. It is defined that for 2 keV and higher the cluster average size increases and it is well approximated by the linear dependence on PKA energy both for interstitials and vacancies.

The obtained results can be used for development of models of radiation damage of Fe–Cr alloys including multi-scale approach.

Acknowledgement

This work has been supported by Helmholtz Gemeinschaft and Russian Foundation for Basic Research in frame of joint research group HRJRG-013. The activities are supported by the nuclear Fusion Programme of Forschungszentrum Karlsruhe.

References

[1] C. Petersen, V. Shamardin, A. Fedoseev, G. Shimansky, V. Efimov, J. Rensman, J. Nucl. Mater. 307–311 (2002) 1655.
[2] E. Gaganidze, H.-C. Schneider, C. Petersen, J. Aktaa, A. Povstyanko, V. Prokhorov, R. Lindau, E. Materna-Morris, A. Möslang, E. Diegele, R. Lässer, B. van der Schaaf, E. Lucon, in: Proceedings of the 22nd IAEA Fusion Energy Conference, 13–18 October 2008 Geneva, Switzerland (Paper FT/P2-1).
[3] L. Malerba, D. Terentyev, P. Olsson, R. Chakarova, J. Wallenius, J. Nucl. Mater. 329–333 (2004) 1156.
[4] D.A. Terentyev, L. Malerba, R. Chakarova, K. Nordlund, P. Olsson, M. Rieth, J. Wallenius, J. Nucl. Mater 349 (1) (2006) 119.
[5] J. Wallenius, P. Olsson, C. Lagerstedt, N. Sandberg, R. Chakarova, V. Pontikis, Phys. Rev. B 69 (2004) 094103.
[6] J.-H. Shim, H.-J. Lee, B.D. Wirth, J. Nucl. Mater. 351 (2006) 56.
[7] A.N. Balashov, M. Yu Tikhonchev, E.I. Shamarina, G.A. Shimansky, M.V. Musina. Molecular Dynamic Method of Calculations of Primary Radiation Damage, Interaction and Properties of Point Defects in Multicomponent Materials. Preprint TSTU, Tver, 2000 (in Russian).
[8] M.S. Daw, M.I. Baskes, Phys. Rev. B 29 (1984) 6443.
[9] M.F. Finnis, J.E. Sinclair, Philos. Mag. A 50 (1984) 45.
[10] V. Rosato, M. Guellopé, B. Legrand, Philos. Mag. A 59 (2) (1989) 321.
[11] K. Nordlund, Molecular Dynamics: Introduction, International School on Modelling of Irradiation Damage, Auberge de la Ferme, Rochehaut, Belgium, 1–5 October 2007 (collected lectures on CD).
[12] G.J. Ackland, M.I. Mendelev, D.J. Srolovitz, S.W. Han, A.V. Barashev, J. Phys. Condens. Matter. 16 (2004) S2629.
[13] M.I. Mendelev, S. Han, D.J. Srolovitz, G.J. Ackland, D.Y. Sun, M. Asta, Philos. Mag. 83 (2003) 3977.
[21] P. Ehrhart, K.H. Robrock, H.R. Schober, in: R.A. Johnson, A.N. Orlov (Eds.), Physics of Radiation Effects in Crystals, Elsevier, Amsterdam, 1986, p. 7.
[22] J. Wallenius, P. Olsson, C. Lagerstedt, N. Sandbers, R. Chakarova, V. Pontikis, Phys. Rev. B. 69 (2004) 094103.
[23] K. Katahara, M. Nimalendran, M. Manghnani, E. Fischer, J. Phys. F: Met. Phys. 9 (1979) 2167.
[24] P. Vajda, Rev. Mod. Phys. 49 (3) (1977) 481.
[25] M. Hohenstein, A. Seeger, W. Sigle, J. Nucl. Mater. 169 (1989) 33.
[26] F. Maury, P. Vajda, M. Biget, A. Lucasson, P. Lucasson, Radiat. Effects 25 (3) (1975) 175.
[27] K. Nordlund, J. Wallenius, L. Malerba, Nucl. Instrum. Meth. Phys. Res. B 246 (2) (2006) 322.
[28] F. Maury, M. Biget, P. Vajda, A. Lucasson, P. Lucasson, Phys. Rev. B 14 (12) (1976) 5303.
[29] J.N. Lomer, M. Pepper, Philos. Mag. 16 (144) (1967) 1119.
[30] P.G. Lucasson, R.M. Walker, Phys. Rev. 127 (2) (1962) 485.
[31] T.E. Mitchell, G. Das, A. Kenik, in: Paper Presented at the International Conference on the Fundamental Aspects of Radiation Damage in Metals, Gatlinburg, Tenn., USERDA Conf. – 751006-P1, 1975, p. 73.
[32] M. Biget, F. Maury, P. Vajda, A. Lucasson, P. Lucasson, 1977 (unpublished).
[33] ASTM E521, (E521-89) Practice for Neutron Radiation Damage Simulation by Charged-Particle Irradiation. Annual Book of ASTM Standards, vol. 12.02, 1995.
[34] T. Konishi, K. Ohsawa, H. Abe, E. Kuramoto, Comput. Mater. Sci. 14 (1999) 108.
[35] P. Olsson, I. Abrikosov, L. Vitos, J. Wallenius, J. Nucl. Mater. 321 (2003) 84.
[36] C. Domain, Quoted in Olsson et al., SCK-CEN-BLG-950, 2002 (private communication).
[37] D. Farkas, C. Schon, M. de Lima, H. Goldstein, Acta Mater. 44 (1996) 409.
[38] D.J. Bacon, A.F. Calder, F. Gao, Radiat. Effects Def. Sol. 141 (1997) 283.
[39] S.J. Wooding, D.J. Bacon, W.J. Phythian, Philos. Mag. A 72 (1995) 1261.
[40] J.P. Biersack, J.F. Ziegler, Nucl. Instrum. Meth. 141 (1982) 93.